Journal Pre-proofs

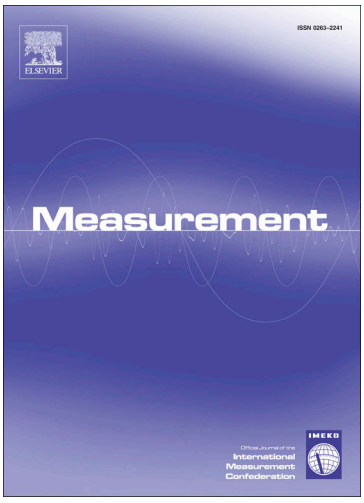

Contactless magnetic nanoparticle detection platform based on non-linear GMI effect

Juan Jesús Beato-López, José María Algueta-Miguel, Cristina Gómez-Polo

PII: S0263-2241(21)00576-5
DOI: https://doi.org/10.1016/j.measurement.2021.109602
Reference: MEASUR 109602

To appear in: *Measurement*

Received Date: 15 March 2021
Revised Date: 23 April 2021
Accepted Date: 12 May 2021

Please cite this article as: J. Jesús Beato-López, J. María Algueta-Miguel, C. Gómez-Polo, Contactless magnetic nanoparticle detection platform based on non-linear GMI effect, *Measurement* (2021), doi: https://doi.org/10.1016/j.measurement.2021.109602

Contactless magnetic nanoparticle detection platform based on non-linear GMI effect

Juan Jesús Beato-López [a,b]*, José María Algueta-Miguel [c,d] and Cristina Gómez-Polo [a,b].

[a] Departamento de Ciencias, Universidad Pública de Navarra, 31006 Pamplona, Spain

[b] Institute for Advanced Materials and Mathematics INAMAT², Universidad Pública de Navarra, 31006 Pamplona, Spain

[c] Departamento de Ingeniería de Electricidad, Electrónica y Comunicación, Universidad Pública de Navarra, 31006 Pamplona, Spain

[d] Institute of Smart Cities, Universidad Pública de Navarra, 31006 Pamplona, Spain

[*] Corresponding author: Juan Jesús Beato-López (juanjesus.beato@unavarra.es)

Abstract

A detection platform based on non-linear Giant Magnetoimpedance Effect was analyzed for the design of a contactless and low-cost detector of magnetic nanoparticles. The sensor consists of two soft magnetic amorphous wires ($Co_{66}Fe_2Si_{13}B_{15}Cr_4$, 1.5 cm in length) placed in parallel and connected electrically in series. Initially, a simple voltage divider was employed to characterize the variations of the first, V_{1f} and second harmonic, V_{2f}, voltages. Their response was analyzed under the effect of the remnant magnetic field generated by different amounts of Fe_3O_4 nanoparticles (mean diameter 140 nm) as a function of an external magnetic field, H. Due to the larger relative variations showed by V_{2f}, the second harmonic was chosen for the final prototype development. An electronic interface was designed for both current excitation and V_{2f} detection. The designed detection platform, characterized by high detection sensitivity, low-cost, portable, and reusable features, can be employed to efficiently detect magnetic nanoparticles.

Keywords: Giant Magnetoimpedance, magnetic sensors, magnetic nanoparticles, contactless detection platform, electronic interface, sensitivity.

1. Introduction

Nanomaterials have attracted the attention of the technological and scientific sectors during the last decades. This interest relies on the variation of the chemical and physical properties with respect to the bulk material as a result of the diminution of their size [1]. In this sense, magnetic nanoparticles (MNPs) have turned a very attractive tool as a result of the combination of their excellent properties (small size, physicochemical stability, biocompatibility, low toxicity, environmental friendly response, and low cost of production [2]–[4]) and the interaction with external magnetic fields that enables their remote control through the induction of translations, rotations, or even the generation of heat [5]. This remarkable combination of properties allows their potential use in relevant fields, namely biomedicine (magnetic biosensing, magnetic imaging, drug and gene delivery, magnetic resonance imaging, hyperthermia) [6] environmental applications (pollutant removal, toxicity mitigation) [7], [8], catalysis [9] and data storage [10] among others. Besides, the magnetic nature of these particles enables their detection and/or quantification through the use of magnetic sensors [11]. As a consequence of this wide use, the necessity of designing low-cost, fast time response and high sensitive MNPs detectors is getting more and more relevant.

Different techniques have been proposed for the design of high-sensitivity MNPs detectors, explicitly inductive sensors [12], [13], magnetoresistive sensors (MR) [14]–[17], Hall sensors [18], [19], spin-valve sensors [20], superconducting quantum interference devices (SQUID) [21], etc. Special attention must be paid in the biosensing field, where the most exigent conditions take place due to the low concentrations of the detectable target, usually composed of a composite (analyte or biological agent specifically bound to the ad-hoc functionalized MNPs´ surface [22]). In this sense, SQUID-based devices exhibit the largest sensitivity. However, the drawbacks related to the necessity of employing cryogenic liquids (helium and/or nitrogen) hinder their massive use [18]. At this point, the Giant Magnetoimpedance effect (GMI) has been revealed as a useful tool for the design of highly sensitive MNPs detectors and biosensors because of their quick response, smaller size, higher stability, low cost [23], and especially the larger sensitivity to low magnetic fields [24] when compared to the techniques previously indicated.

The GMI effect can be defined as the huge variations experimented by the high-frequency electrical impedance, Z, of a ferromagnetic conductor under the effect of an external *DC* magnetic field, H [25]. These variations can be understood within the framework of the classic electrodynamics theory, where the impedance changes can be correlated to the variations experimented by the skin depth, $\delta = \delta(\mu) = \sqrt{1/\pi f \sigma_c \mu}$ (μ is the magnetic permeability, σ_c is the conductivity of the material and f the driving frequency) through its functional dependence with μ. So, the application of an external magnetic field modifies μ and consequently $\delta(\mu)$ leading to measurable changes in Z. Under this principle, high-sensitive magnetic detectors have been already proposed in the bibliography [23], [26], [27].

Different GMI MNPs detectors have been proposed based on amorphous ribbons [24], wires [28], microwires [29] and thin-film layers [30], [31]. More recently, some devices for the remote detection of MNPs have also been proposed to explore the possibility of in vivo applications. This step requires larger sensitivities than usually are accompanied by more complex prototypes and/or signal processing [32]. Thus, sensors capable of detecting distant MNPs embedded in ferrofluids [33], or solid structures [32] have been proposed. In general, the application of an external field is required to partially magnetize the detectable target, causing a decrease in the detection capacity of the sensing element. In the context of the continuous searching of larger sensitivity devices, previous works have explored the possibility of the higher capacity of detection of the non-linear GMI effect. Generally speaking, when low amplitude current intensities are applied, the GMI response remains linear. However, at larger intensities, a nonlinear response may appear, leading to the existence of higher harmonics in the GMI voltage. Focusing on the second harmonic voltage, V_{2f}, a larger sensitivity respecting the fundamental or first harmonic voltage, V_{1f} has been reported in the vicinity of zero external *DC* magnetic field [34], [35]. These second harmonic GMI devices are based on the asymmetrical magnetization process experienced by a high permeability ferromagnetic core. Although this working principle is similar to (coil-less) fluxgate sensors [36], some differences can be stated between them. Coil-less fluxgate sensors usually work under lower frequency than those based on the GMI effect [37], giving, as a result, a negligible role of the resistance in the fluxgate sensor output [38] in contrast with the relevance exhibited in the GMI sensors. Anyway, we previously analyzed the V_{2f} detection capacity for the superparamagnetic MNPs detection (Fe_3O_4) [39], [40] where the larger detection capacity of V_{2f} was demonstrated. Nevertheless, the detection of these nanoparticles required the application of high magnetic fields, H, during the detection process causing a noticeable diminution in the sensitivity of the sensor itself. As a result, a direct contact nanoparticle-sensor was required, hindering a contactless detection procedure.

Although these superparamagnetic Fe-based particles (1-50 nm) play an important role in the sensing field, larger MNPs in size (100- 500 nm) are also successfully employed in the development of high sensitivity sensors and biosensors [41] [42], [43].

Accordingly, the present work aims to analyze whether the reported better performance of V_{2f} could be extended to larger ferrimagnetic Fe_3O_4 (non-superparamagnetic) particles, characterized by magnetic hysteresis and remnant magnetization. In this way, when the external H field is removed, a remnant magnetic field, B_{rem}, remains, enabling the detection (and quantification) of the MNPs even in absence of H. So, a direct comparison of V_{1f} and V_{2f} MPNs detection capacity is performed for its potential application in the design of new magnetic sensors and biosensors with enhanced sensitivity. A GMI sensor composed of two soft magnetic amorphous wires ($Co_{66}Fe_2Si_{13}B_{15}Cr_4$, 1.5 cm in length) were submitted to the remnant field generated by different amounts of Fe_3O_4 nanoparticles (mean diameter 140 nm) fixed on glass substrates. The employed configuration enabled the analysis of $V_{1f}(H)$ and $V_{2f}(H)$ as a function of the mean distance MNPs-sensor. The results confirm the highest MNPs sensitivity of the V_{2f}. The superior detection capacity was further analyzed to design a high sensitivity MNPs detection platform capable to detect and quantify low amounts of MNPs at large distances (order of mm) under the principles of low cost, simple design (the external magnetic field is not required), single-step measurement process, and reusability, easing the detection process. So, the proposed sensor enables the detection process respecting others GMI detectors at the time that offers a larger spatial resolution where MNPs can be detected.

2. Materials and Methods

2.1 Magnetic nanoparticles

Commercial Iron Oxide, Fe_3O_4, magnetic nanoparticles (MNPs) were employed as the detectable magnetic target (Sigma Aldrich company, 637106-25G). The particle average size estimation has been obtained from the Transmission Electron Microscopy (TEM) measurements performed in an "FEI TECNAI T20" microscope. A mean diameter of 140 ± 50 nm was obtained (Figure 1a). Initially, different masses, *m*, of magnetic nanoparticles, ranging from 1 to 15 mg were diluted in 0.2 mL of distilled water. Then, every solution was deposited onto a square-shaped cover glass (in the following *holder*) with $a = 12\ mm$ side and $d_0 = 0.2\ mm$ thickness. Thus, a set of MNPs supported on the glass holders was prepared for their detection. Table 1 summarizes the characteristics for each prepared sample, where the superficial density, $\sigma = {}^{m}/_{S}$, was introduced since the samples were spread over the whole holder area ($S = a^2$).

Table 1. Set of MNPs samples prepared for detection: MNP mass, *m*, and superficial density, *σ*.

Sample	**S1**	**S2**	**S3**	**S4**
m (mg)	1	3	5	15
$\sigma({}^{mg}/_{mm^2})$	0.007	0.021	0.035	0.104

During the evaporation of water solvent, a constant *DC* magnetic field of H_{elec} = 0.4 T generated by an electromagnet (Applied Magnetics Laboratory, 4H2-45), was applied to favor the alignment of the magnetic nanoparticles. After the total evaporation of the aqueous solution, the MNPs displayed a remnant magnetic field, $B_{rem} = \mu_0 M_r$ (M_r: remnant magnetization)

although the removal of H_{elec}. Figure 1b shows the hysteresis loop measured with a SQUID magnetometer (MPMS-XL, Quantum Design) under a maximum applied field of 0.4 T. The non-zero value of the remnant magnetization is clearly visible as a consequence of the large mean nanoparticle size (above the superparamagnetic critical size). The presence of B_{rem} would enable the detection of the MNPs through the changes underwent by the electrical impedance, Z, of the Giant Magnetoimpedance (GMI) sensor.

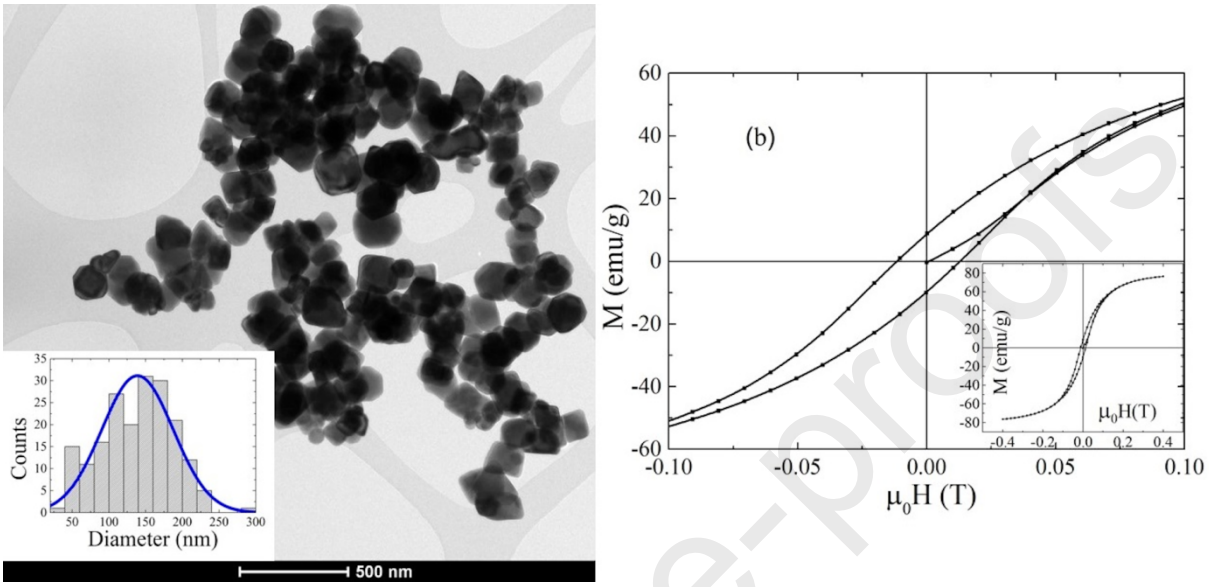

Figure 1: a) TEM micrographs and size distribution of MNPs. b) Room temperature hysteresis loop (*M-H*) of the magnetic nanoparticles. As the inset shows, the maximum applied magnetic field was 0.4T.

2.2 Sensor design

The sensing element configuration is schematically shown in Figure 2. Two parallel amorphous wires obtained by the in-rotating-water quenching technique [44] (composition $Co_{66}Fe_2Si_{13}B_{15}Cr_4$), 1.5 cm in length and 90 μm of diameter, were fixed on a flat plastic substrate and connected electrically in series through copper (Cu) connecting terminals. Such configuration enables the enlargement of the effective detecting surface of MNPs in comparison to a single wire element. Two supports identical to the one used for nanoparticle deposition were attached to both sides of the wires. Thus, the MNPs samples could be placed over the magnetic wires at a controlled distance, d (see Figure 2).

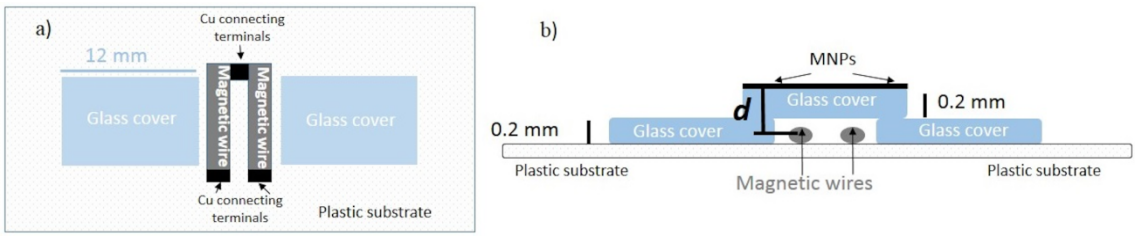

Figure 2. a) Top and b) cross-view of the detection configuration.

2.3 Sensor characterization and MNPs detection

Since the principle of detection is based on the GMI effect, the first step was to establish the conditions to optimize it. Thus, the sensor was placed at the center of a pair of Helmholtz coils that generates a uniform *DC* magnetic field, H, ($H = \left(583\,\frac{Am^{-1}}{A}\right)I(A)$; I: electric current coil of radius $R = 4.5cm$) along the axis of the wires. Simultaneously, the sensor was excited employing a standard signal generator (Standford Research Systems DS 345) with a sinusoidal *AC* signal whose amplitude was measured with an *AC* current probe (Tektronix P6021). The variations of impedance, Z, namely impedance variation ratio ($\frac{\Delta Z}{Z}(\%) = \frac{Z(H_{MAX}) - Z(H=0)}{Z(H_{MAX})} x100$), in the absence and presence of a magnetic field $H_{MAX} = 3.8\ kA/m$, were registered with a commercial lock-in amplifier (Standford Research Systems SR 844) as a function of the exciting current frequency (ranging from 100 kHz to 1 MHz) using a *voltage divider* configuration (Figure 3a). Optimal conditions (maximum $\frac{\Delta Z}{Z}(\%)$ ratios) were found for $f = 100\ kHz$ and $I_{pp} = 15\ mA$. These conditions remained constant during the MNPs detection experiments.

Regarding MNPs detection procedure, the variations of the first, V_{1f}, and the second harmonic, V_{2f} components of the GMI voltage of the sensor were evaluated as a function of *H* employing the described voltage divider configuration (under sinusoidal or triangular current excitation). The changes in V_{1f} and V_{2f} were analyzed as a function of the amount of nanoparticles on the glass substrate (Table 1) and for different values of *d*. The minimum distance ($0.31\ mm$) corresponds to the situation shown in Figure 2b. From this minimum distance, empty glass holders were intercalated between the sensing wires and the MNPs, increasing d in an integer multiple value of d_0 = 0.2 mm. Furthermore, both V_{1f} and V_{2f} were comparatively analyzed submitting the holder to a rotation of $180°$. Under this rotation ($\alpha = 180°$), B_{rem} reverses its direction with respect to the intial non rotated state ($\alpha = 0°$).

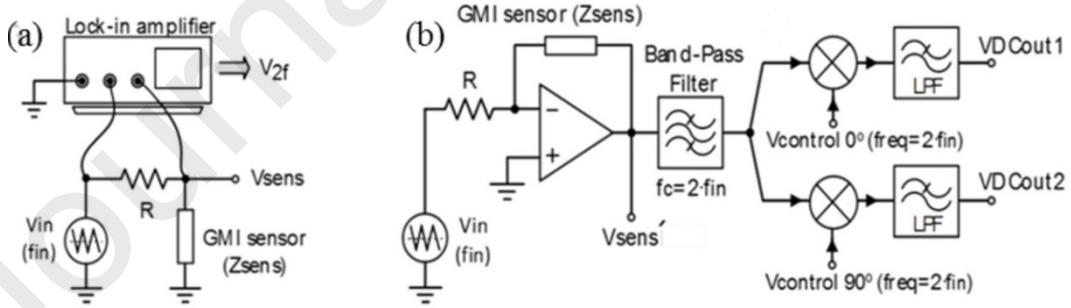

Figure 3. Functional block diagram of the employed electronics: (a) Voltage divider configuration for laboratory sensor characterization and (b) Proposed electronic design for the sensor.

2.4 Electronics

In the designed electronic interface (see Figure 3b), a triangular excitation current is applied to the sensor, which is placed in the feedback loop of a transimpedance amplifier. In contrast to the inherent non-linear response of the voltage divider configuration where $V_{sens} = V_{in} \cdot Z_{sens}/($

$Z_{sens}+R$), the transimpedance amplifier of Figure 3b leads to a voltage signal $V_{sens'} = (V_{in}/R)$ Z_{sens} linear with the sensor impedance ($Z = Z_{sens}$), also increasing the sensitivity significantly (see section 3. Results and discussion for more details). Finally, an *implemented "two-phase lock-in amplifier"* provides two output *DC* voltages which are proportional to the phase and quadrature components of the second harmonic voltage V_{2f} respectively. The proposed electronics was employed for the MNPs detection at null magnetic field and to characterize the spatial range, d where they where detecteable.

3. Results and discussion

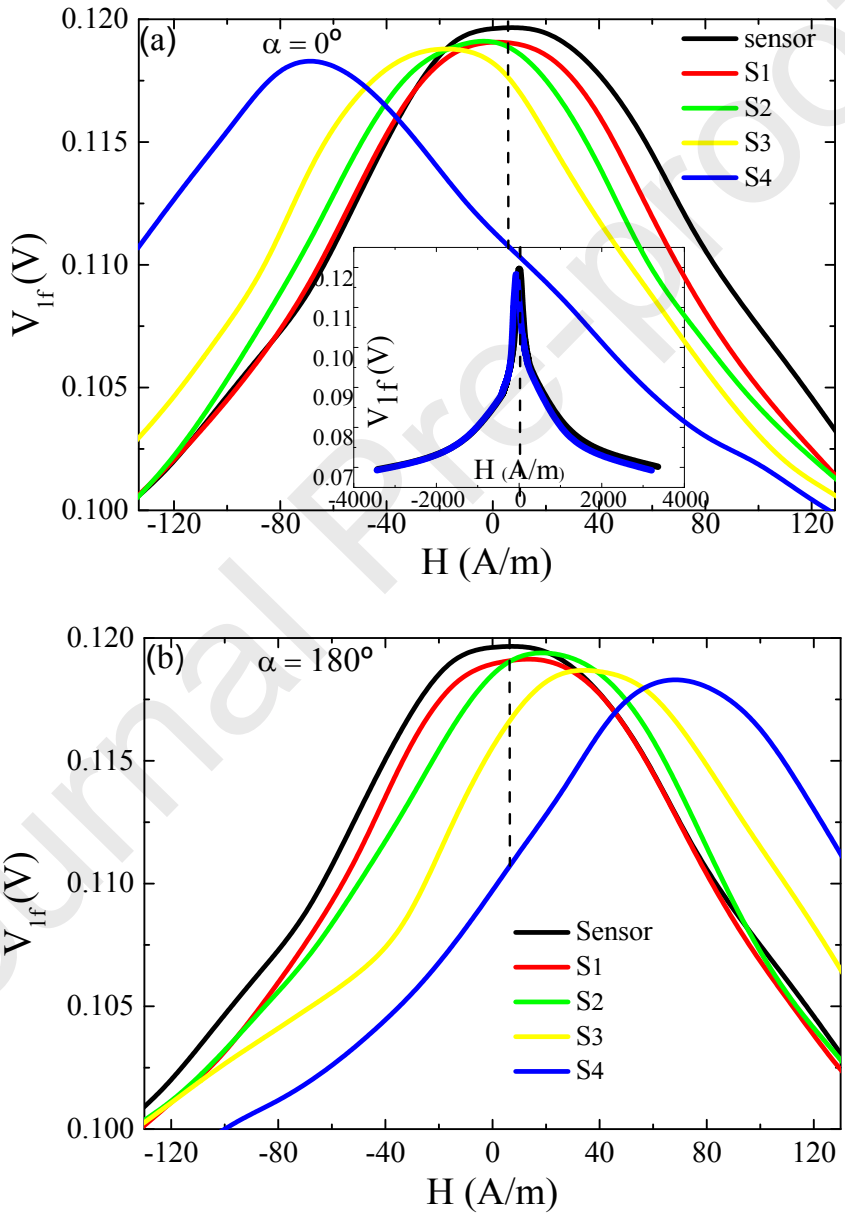

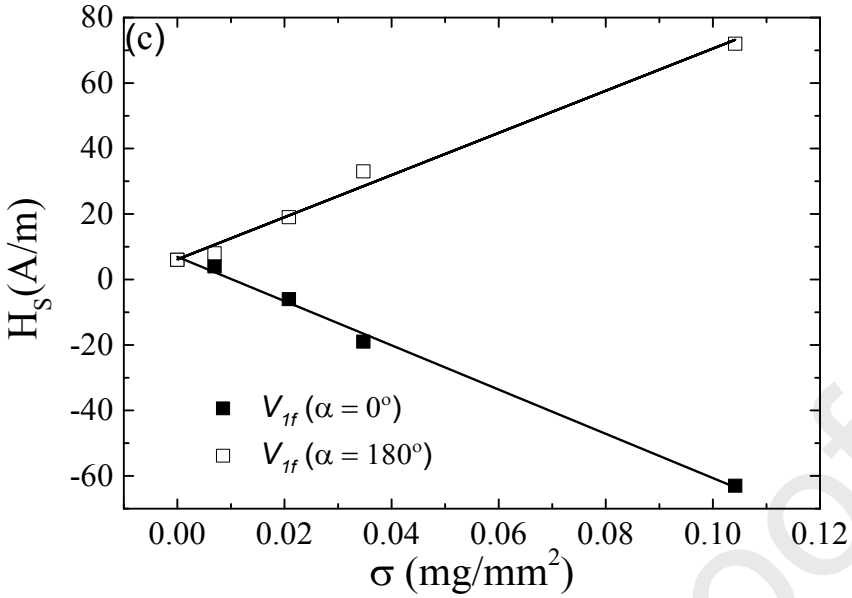

Figure 4. Variation of the first harmonic voltage, V_{1f} with the applied magnetic field, *H*, for the set of MNPs samples, S1, S2, S3, and S4 ($\sigma = 0.007, 0.0021, 0.0035$ and $0.104\,{}^{mg}/_{mm^2}$ respectively) for a rotation angle (a) $\alpha = 0°$ and (b) $\alpha = 180°$; (c) H_S field for maximum V_{1f} under both configurations. Inset: (a) V_{1f} versus *H* for the *sensor* and under the presence of *S4* sample, $\sigma = 0.104\,{}^{mg}/_{mm^2}$.

Firstly, the evolution of V_{1f} as a function of *H* under the effect of the set of MNPs samples (see Table 1) was examined. As an example, the inset of Figure 4a shows the evolution of V_{1f} with *H* for the *sensor* (without MNPs) and in the presence of S4 sample ($\sigma = 0.104\,{}^{mg}/_{mm^2}$). The *sensor* response displays the characteristic GMI curve of soft magnetic nearly zero magnetostrictive wires, where the lack of a clear intrinsic magnetoelastic anisotropy has associated a not well-defined domain structure of the wires. This situation leads to a single peak behavior at the excitation frequency, 100 kHz, around $H \approx 0$ (maximum impedance) and a sharp decrease in V_{1f} as *H* increases, up to reach an almost constant (saturation) voltage. The presence of the MNPs gives rise to a shift in the curve towards negative *H* values, reaching V_{1f} a maximum value for the S4 sample at $H \approx$ -63 A/m. The shift in the curves can be clearly seen in Figure 4a, where $V_{1f}(H)$ is plotted in the low *H* region for the set of analyzed MNPs. As σ increases, the displacement towards negative *H* values is enhanced. A symmetrical behavior was found when the sample holder (and thus the aligned MNPS) was rotated at an angle α = 180°. That is, similar shifts but in opposite direction (towards positive *H*) were produced when the sensor was under the effect of rotated MNPs (see Figure 4b). The curve shifts can be easily quantified by the change of the *H* field (H_S) at which the voltage V_{1f} shows the maximum value. As can be seen in Figure 4c, H_S linearly depends on σ, leading to analogous slope values under both configurations $-6.8 \pm 0.3x10^{-4}$ and $6.4 \pm 0.4x10^{-4}\,{}^{Am^{-1}}/_{mg}$ for α = 0° (non-rotated) and 180°, respectively. This fact indicates that the sensor is not only sensitive to the intensity of the magnetic field generated by the MNPs but also to its direction. No less important is the circumstance that the shifts take place in the whole *H* interval and maintaining almost constant the relative variation of impedance, $\frac{\Delta Z}{Z}(\%)$, in all cases. Consequently, this behavior can be attributed to the effect of a constant magnetic field acting on the sensor associated with the remnant magnetic field generated by the MPNs, B_{rem}. Thus, the sensor performance can be analyzed in terms of an effective magnetic field, H_{eff}, $H_{eff} = H \pm H_{MNPs}$, where $H_{MNPs} \propto$

B_{rem}/μ_0 is the magnetic field associated to the remnant magnetization of the MNPs and it must be subtracted or added depending on the rotation angle (α = 0° and 180°, respectively). So, for $H_{eff} = 0$, maximum and minimum values in V_{1f} and V_{2f}, correspondingly, are achieved for $H_S = -H_{MNPs}$, (α = 0°) and $H_S = H_{MNPs}$,(α = 180°). At this point, it must be noted that the *sensor* response (without MNPs) displays the maximum value at $\sim 6\,A/m$. This fact may be attributed to the effect of small parasitic magnetic fields (i.e Earth magnetic field) during the acquisition of the measurements.

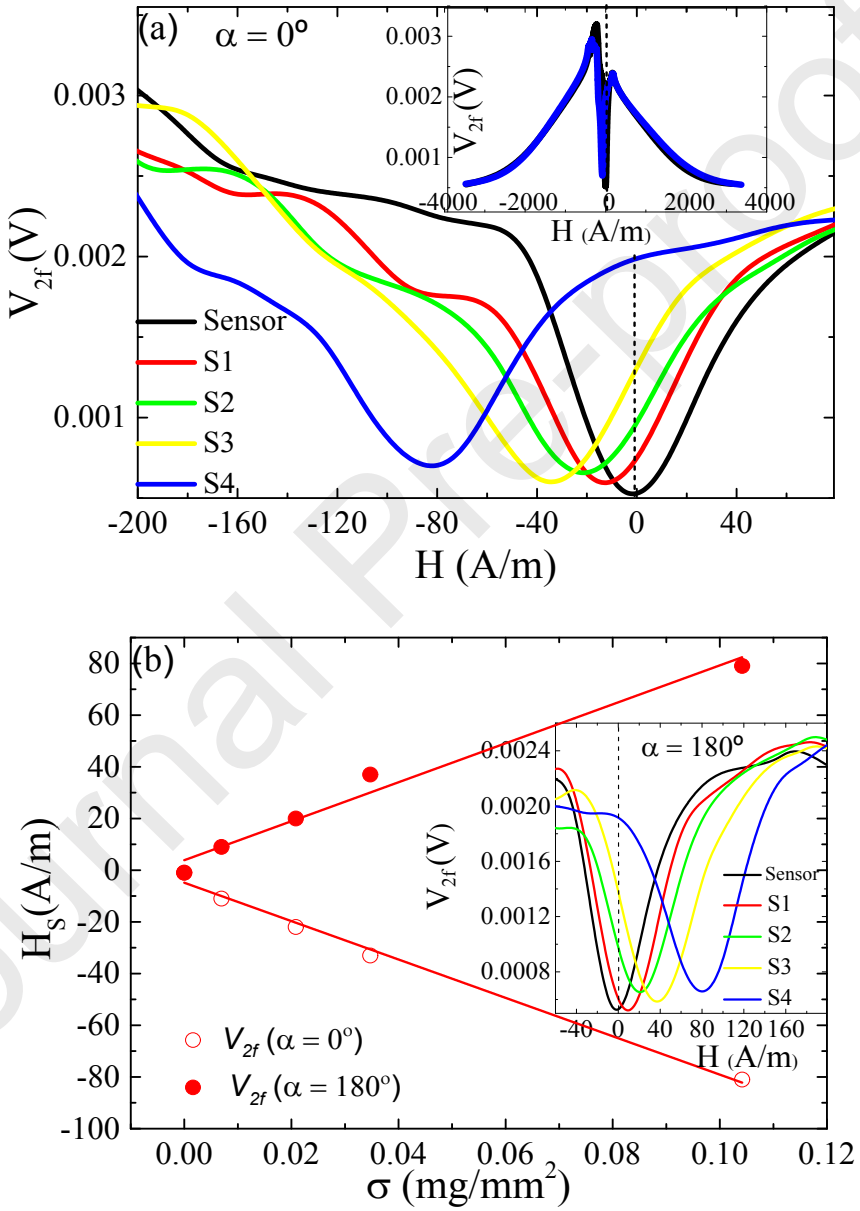

Figure 5. Variation of the second harmonic voltage, V_{2f} with the applied magnetic field, *H* for the set of MNPs S1, S2, S3, and S4 (σ = 0.007, 0.0021, 0.0035 and $0.104\,mg/mm^2$ respectively), (a) at a rotation angle $\alpha = 0°$ and (b) H_S field at minimum V_{2f} under both configurations. The insets show (a) the curves obtained for the *sensor* and S4 in the whole *H* interval and (b) V_{2f} versus *H* for rotated $\alpha = 180°$ MNPs.

Regarding the second harmonic response, Figure 5 exhibits the evolution of V_{2f} as a function of *H* under the effect of increasing σ. Equally, the inset in this figure shows $V_{2f}(H)$ for the *sensor* (without nanoparticles) and under the effect of the S4 sample ($\sigma = 0.104\,{}^{mg}/_{mm^2}$). As it has been previously reported [45], [46] V_{2f} displays a minimum value when $H_{eff} = 0$. Analogously to V_{1f}, V_{2f} shifts towards negative and positive *H* values for α = 0° (Figure 5a) and 180° (Inset of Figure 5b), respectively, under the presence of MNPs. Furthermore, as Figure 5b displays, a similar linear trend with σ is found in the applied magnetic field at which V_{2f} is minimum, H_s, with slopes $(-7.4 \pm 0.4)x10^{-4}$ and $(7.4 \pm 0.6)x10^{-4}\,{}^{Am^{-1}}/_{mg}$ for α = 0° and 180°, respectively. Also, in this case, a non-zero H_S value is detected for σ= 0. These results are further confirmed in Figure 6, where direct comparison of the H_s values for both V_{1f} and V_{2f} are plotted as a function of σ for non-rotated MNPs (α = 0°). Besides, the curves obtained reveals the linear relationship between H_{MNPs} and the amount of MNPs, indicating the negligible formation of MNPs clusters or aggregates within the analyzed interval.

Nevertheless, regarding practical purposes, the determination of H_S does not enable the design of a simple MNPs detection procedure. Conversely, the voltage changes can be employed to easily characterize the presence of MNPs. To determine the optimum harmonic (higher sensitivity), the variations of V_{1f} and V_{2f} at null applied magnetic field ($H = 0$) were analyzed as a function of σ and d respectively. The results are shown in Figure 7a and Figure 7b where the rotated MNPs voltages were not plotted for the sake of clarity due to the similarity with the non-rotated values. In both cases, a non-linear trend is obtained for both harmonics, preventing the calculation of the sensitivity. Nevertheless, the estimation of the capacity of detection was performed from the calculation of the relative variations underwent by every harmonic, $\left|\left({}^{V_{if}(x) - V_{if}(x_{max})}/_{V_{if}(x_{max})}\right)x100\right|$; where $i = 1,2$; $x = \sigma\ or\ d$, $\sigma_{max} = 0.104\,{}^{mg}/_{mm^2}$ and $d_{max} = 37\ d_0$. V_{2f} exhibits a clear enhancement with almost one order of magnitude higher relative variations (74% and 68%) in comparison with V_{1f}(8% and 5%) for σ and d respectively. Accordingly, V_{2f} was considered for the subsequent studies and the development of the final detection device. However, it is important to stress that both harmonics have demonstrated their capability to detect MNPs without any physical contact between the sensor and the MNPs, enabling the reuse of the detection platform.

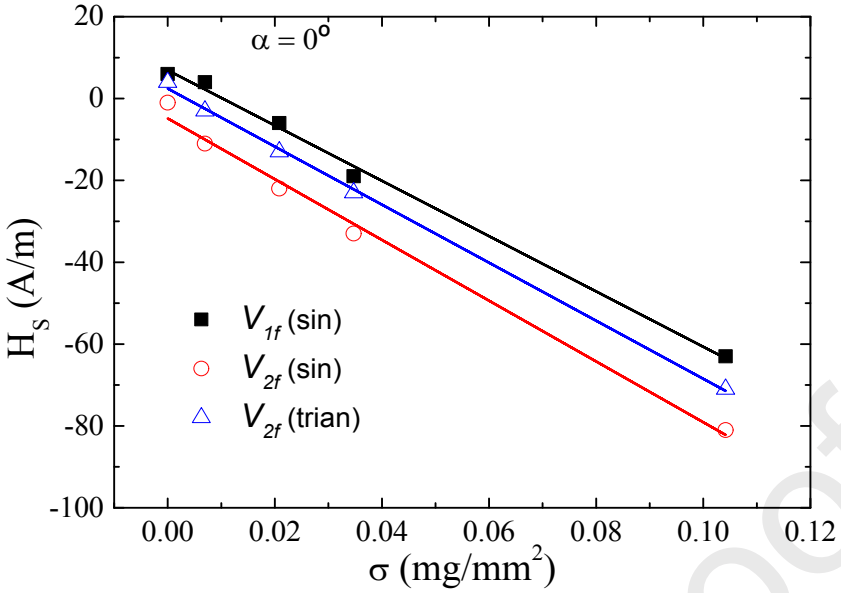

Figure 6. Magnetic field, H_S, for the maximum and minimum in V_{1f} and V_{2f}, respectively, as a function of σ for non-rotated MNPs. In the case of V_{2f} the response was also analyzed under a triangular signal excitation.

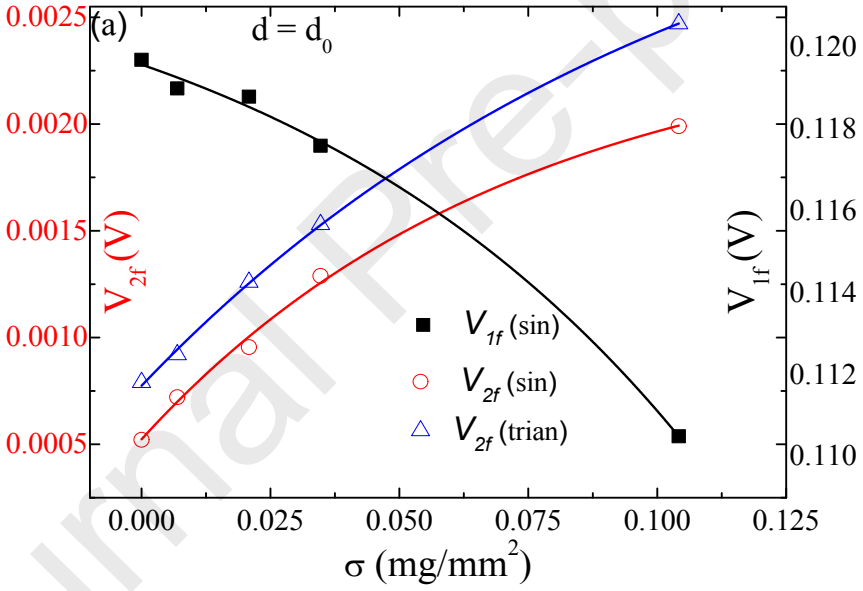

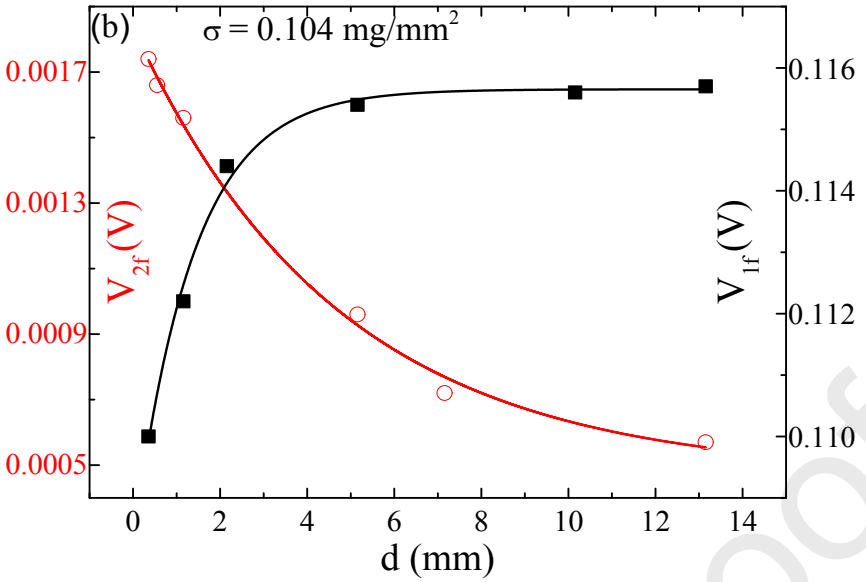

Figure 7. Variation of the first harmonic, V_{1f}, and second harmonic voltage, V_{2f} at $H = 0$ as a function of (a) σ (for a fixed distance $d = d_0$), and (b) d under the effect of the S4 sample.

For practical purposes (electronic interface), the response of V_{2f} was equivalently studied but being excited with a triangular signal. No relevant differences were observed with respect to the sinusoidal excitation (even for V_{1f} not shown in the figure). As can be observed in Figure 6 and Figure 7a, similar sensitivity with σ $(-7.1 \pm 0.1)x10^{-4}\, Am^{-1}/_{mg}$) and maximum relative variation of V_{2f} (68%) at $H = 0$ were obtained, validating so the use of the triangular signal in the final electronic interface.

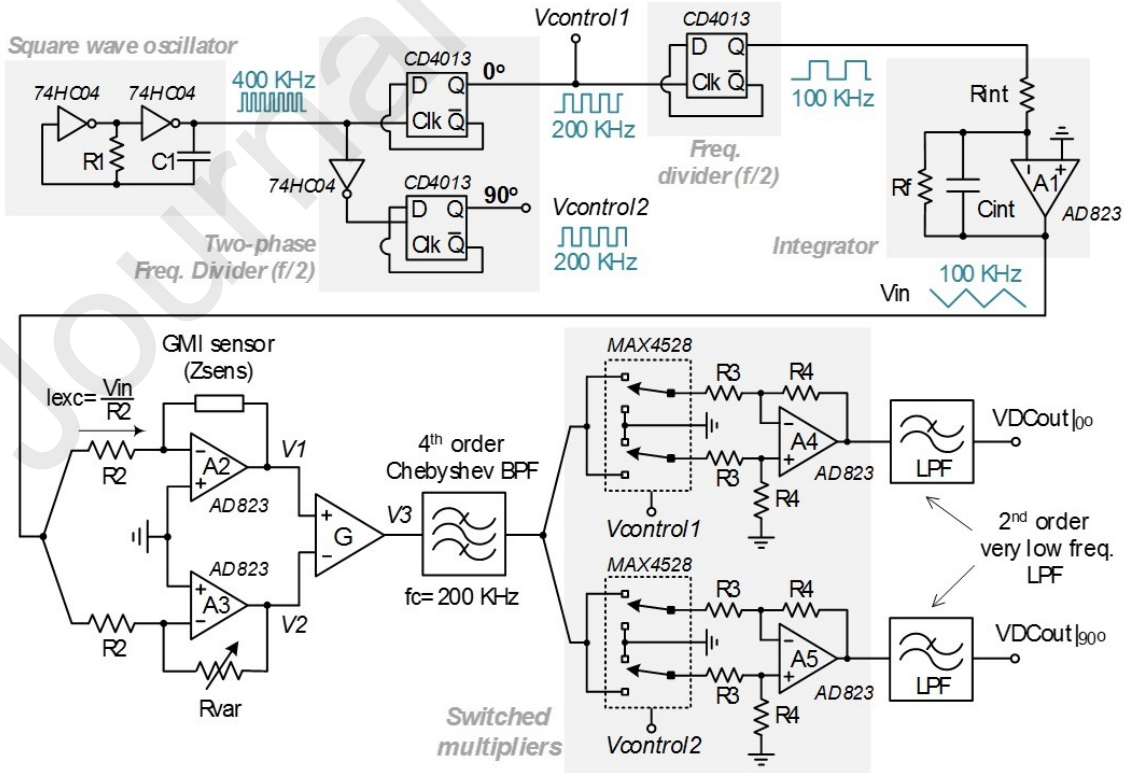

Figure 8. Schematic of the proposed electronic design.

Figure 8 shows the schematic of the developed electronic design for the MNPs detection device. The circuit is feed using a single voltage supply of 5V and a signal ground at 2.5V. The principle of operation of the circuit is as follows: a 400 kHz square-wave oscillator drives a two-phase frequency divider based on D-type flip-flops, generating two 200 kHz square signals with a phase difference of 90° that will be used as reference signals by the "implemented lock-in amplifiers". One of these signals is again frequency-divided and subsequently integrated to obtain the 100 kHz triangular excitation signal V_{in}, so an excitation current V_{in}/R_2 flows through the GMI sensor placed in the feedback loop of a transimpedance amplifier. Thus, a voltage $V_1 = (V_{in}/R_2)Z_{sens}$ is obtained at the output of the amplifier *A2*, where $Z_{sens}$is the impedance of the sensor. It is worth remarking that the voltage V_1 contains all the spectral components of the triangular waveform, whose amplitudes are significantly larger than the small voltage variations introduced by the Z_{sens} changes. For this reason, the additional branch corresponding to the amplifier *A3* and an opamp-based subtractor with a gain *G* has been introduced to enhance the sensitivity to Z_{sens} variations. Note that when the variable resistor *Rvar* is adjusted to the resistive value of the GMI sensor in absence of excitation, a voltage *V2* only differing from *V1* in the non-linearities introduced by the sensor is obtained. Hence, the voltage $V_3 = G(V_1 - V_2)$ will be majorly determined by the Z_{sens} variations. Next, band-pass filtering around the interest frequency of 200 kHz is performed. The resulting signal is applied to a pair of switch-based multiplicators, which introduce a gain factor of *±(R4/R3)* whose sign is controlled by the reference signals *Vcontrol1* and *Vcontrol*2 respectively. Finally, very low-frequency low-pass filters are employed to obtain the output DC voltages $VDCout|0^{\circ}$ and $VDCout|90^{\circ}$, whose root mean square $V_0 = V_{2f} = \sqrt{(VDCout|0^{\circ})^2 + (VDCout|90^{\circ})^2}$ is proportional to the magnitude of the second harmonic generated by the GMI sensor.

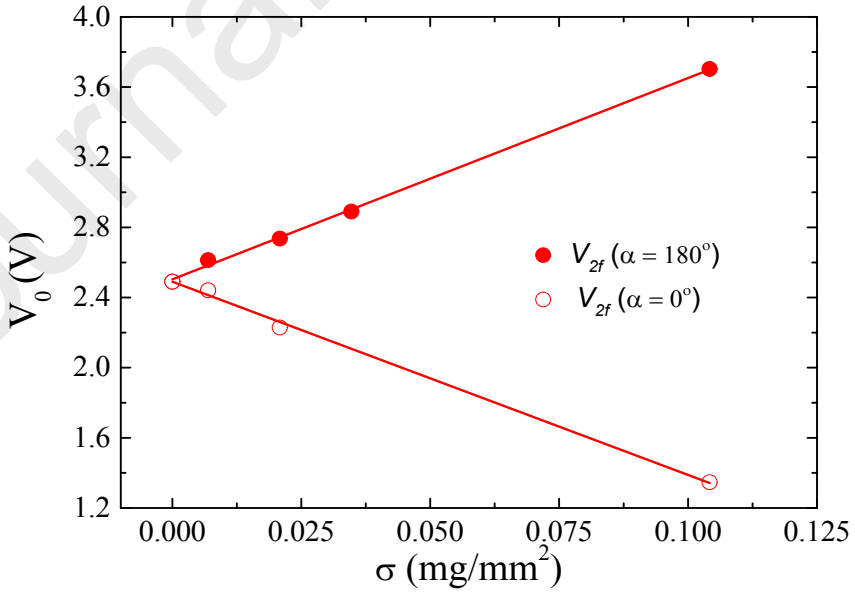

Figure 9. Variation of the second harmonic voltage, V_0 measured by the electronic design at $H = 0$, for varying amount of MNPs, σ, over the sensor.

The first step in the electronic interface implementation was to characterize the capacity of detection of the MNPs through the variations of V_{2f} at $H = 0$ (shown in Figure 9). A linear functional dependence among V_{2f} and σ is obtained. In this sense, the proposed electronic interface employs a transimpedance amplifier configuration that ensures a constant current amplitude ($^{V_{in}}/_{R_2}$) driving the sensor, due to the virtual ground generated at the negative input of *A2*. In consequence, the sensitivity that relates V_{2f} and σ, can be easily calculated from the slope of the curves. As in the previous cases, the similitude in the values of the sensitivity (in absolute value) non-rotated $(-11.0 \pm 0.4)^{V}/_{mg\ mm^{-2}}$, and under 180° rotation, $(11.5 \pm 0.2)^{V}/_{mg\ mm^{-2}}$, validates the accuracy of the measurements.

In addition, the proposed prototype must offer an enhancement in the sensitivity of detection. In this sense, the performance of both experimental setups was compared under similar stimuli, that is, analyzing the distance, d where a fixed amount of MNPs given by $\sigma = 0.007$ and 0.104 $^{mg}/_{mm^2}$ were detectable.

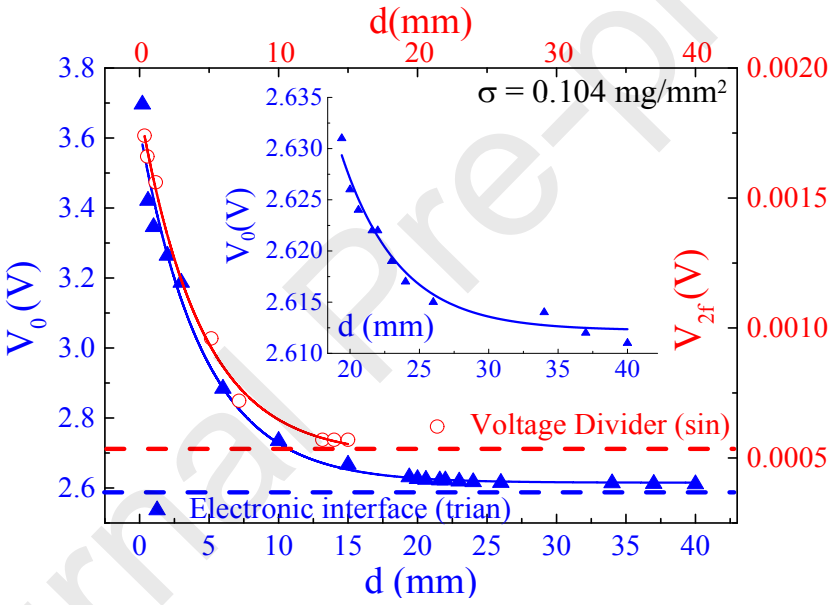

Figure 10. Detected variations of V_0 (second harmonic-electronic interface), as a function of distance d at null magnetic field and $\sigma = 0.104\,^{mg}/_{mm^2}$, ($m = 15mg$) for (-) the electronic interface and (-) V_{2f} voltage divider. Inset: Zoom of the V_{2f} variations for large d values region (electronic interface).

Initially, the highest MNPs density $\sigma = 0.104\,^{mg}/_{mm^2}$ was analyzed. As expected, when the distance between MNPs and sensing wires is increased, V_{2f} decreases towards the value exhibited in the absence of MNPs, depicted in Figure 10 by the respective dashed lines. A clear enlargement of the spatial range of detection (characterized by larger d) is obtained when the electronic interface was employed. The results show a maximum detectable distance close to 13 and 40 mm for the voltage divider and electronic interface, respectively (see inset in Figure 10). Since both systems have been submitted to the same effect of the MNPs (B_{rem}), the improvement in the spatial range of detection can be ascribed to the *ad-hoc* electronics performance. This conclusion is reinforced when the lowest amount of MNPs, $\sigma = 0.007$ $^{mg}/_{mm^2}$, was examined. In this case it was not possible to detect the MNPs under the voltage

divider configuration for distances larger than $2d_0$, while a maximum range of detection close to 5 mm (slightly lower than $25d_0$) was found when the electronic interface was used (see Figure 11).

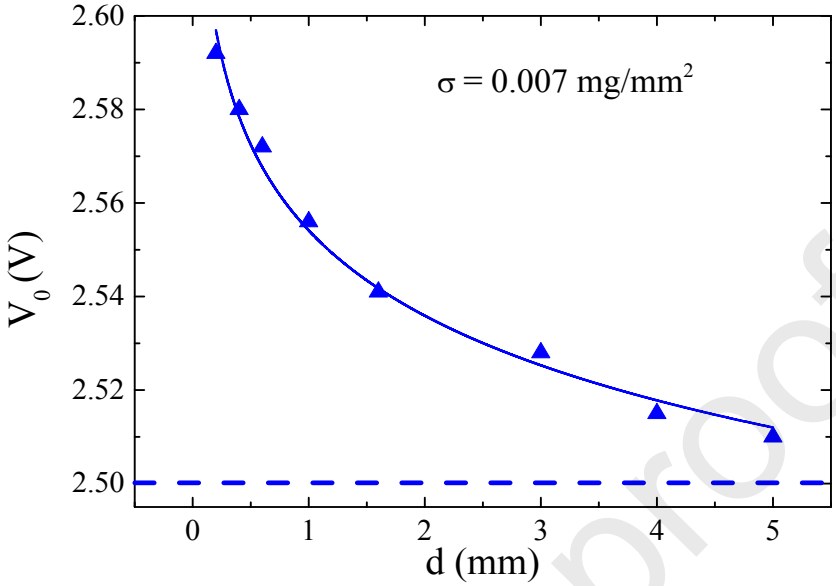

Figure 11. Variations of V_0 (second harmonic-electronic interface) as a function of distance d at null magnetic field and $\sigma = 0.007\,{}^{mg}/_{mm^2}$, ($m = 1mg$) for the electronic interface.

Although the bibliography of MNPs sensors is extensive some comparisons can be established with the proposed sensor. The suggested device is capable to detect micrograms of MNPs, showing the output signal a variation of around 80 ${}^{mV}/_{mg}$ (from the slopes of Figure 9). The lowest analyzed amount (1 mg) was detectable at a maximum distance close to 5 mm, larger than other reported as far as we are concerned. Generally, larger capacities of detection are reported in the bibliography for "on-chip" GMI biosensors [26], [23] [47]. However, these devices are highly specific to the detectable target, hindering their reuse for multipurpose detection. Besides, the complexity of the constituent sensing elements and their experimental setup led to intricate measurement procedures and signal conditioning stages. Similar capacities of detection, are found when compared with other "non-contact systems" [32], [33]. Nevertheless, those systems in general, require more complex device assembly (application of external fields) and signal conditioning systems accompanied by a lower spatial resolution than the proposed device. Thus, the suggested sensor is a trade-off between the large capacity of detection, simple assembly, large spatial resolution, fast and single-step measurement procedure, and low cost of the device from a double perspective, explicitly, the employed sensing element and the substitution of sophisticated measurements systems such as network analyzers, or lock-in amplifiers by a cheap and portable *ad-hoc* electronics.

4. Conclusions

A contactless sensor capable of the detection and quantification of magnetic nanoparticles has been designed. The working principle is based on the variations experimented by the first, V_{1f}, and second harmonic, V_{2f}, voltages of a GMI element composed of two soft magnetic wires ($Co_{66}Fe_2Si_{13}B_{15}Cr_4$, 1.5 cm) in the presence of Fe_3O_4 nanoparticles (mean diameter 140 nm). A

shift of the voltage curves versus the applied *DC* field, *H*, towards negative or positive *H* values is detected depending on the intensity and direction of the remnant magnetic field (stray fields) associated with the magnetic nanoparticles.

At null external magnetic field, V_{2f} experimented relative variations in presence of the MNPs nearly one order of magnitude higher than V_{1f} when both responses were analyzed as a function of σ and d.

An electronic device is proposed for addressing the MNPs detection in a potential final prototype. The proposed electronic interface enables the design of a low-cost and portable device, at the time that enhances the sensitivity of detection displayed by V_{2f}. It can be seen how the spatial range (d) where a fixed amount of MNPs (σ) could be detected was clearly enlarged. The analyzed sensing platform additionally enables the non-contact MNPs detection and thus its reuse for multiple nanoparticle characterization.

CrediT authorship contribution statement

Juan Jesús Beato López: Conceptualization, Methodology, Measurements, Validation, Formal Analysis, Investigation, Data curation, Writing original draft and editing. **José María Algueta Miguel**: Development of electronic interface, Writing review, and editing. **Cristina Gómez Polo**: Conceptualization, Methodology, Formal Analysis, Data curation, Supervision, Resources, Funding acquisition, Writing review and editing.

Declaration of conflicting interests

The authors declare that they have no competing financial interests or personal relationships that could have appeared to influence the work reported in the paper.

Acknowledgments

The work has been performed within the framework of the project MAT 2017-83631-C3-2R (Spanish Ministerio de Ciencia e Innovación) and AEI/FEDER (grant PID2019-107258RB-C32). The soft magnetic wire was kindly provided by Dr. A. Mitra, from NDE & Magnetic Materials Group, CSIR-National Metallurgical Laboratory, Jamshedpur 831007, India. The authors would also like to acknowledge the use of "Servicio General de Apoyo a la Investigación-SAI", Universidad de Zaragoza for the TEM microscopy service.

Bibliography

[1] E. Roduner, "Size matters: why nanomaterials are different," *Chem. Soc. Rev.*, vol. 35, no. 7, pp. 583–592, Jun. 2006, doi: 10.1039/B502142C.

[2] A. Akbarzadeh, M. Samiei, and S. Davaran, "Magnetic nanoparticles: preparation, physical properties, and applications in biomedicine," *Nanoscale Res Lett*, vol. 7, no. 1, p. 144, Feb. 2012, doi: 10.1186/1556-276X-7-144.

[3] L. H. Reddy, J. L. Arias, J. Nicolas, and P. Couvreur, "Magnetic Nanoparticles: Design and Characterization, Toxicity and Biocompatibility, Pharmaceutical and Biomedical

Applications," *Chem. Rev.*, vol. 112, no. 11, pp. 5818–5878, Nov. 2012, doi: 10.1021/cr300068p.

[4] T. A. P. Rocha-Santos, "Sensors and biosensors based on magnetic nanoparticles," *TrAC Trends in Analytical Chemistry*, vol. 62, pp. 28–36, Nov. 2014, doi: 10.1016/j.trac.2014.06.016.

[5] S. Savliwala *et al.*, "Chapter 13 - Magnetic nanoparticles," in *Nanoparticles for Biomedical Applications*, E. J. Chung, L. Leon, and C. Rinaldi, Eds. Elsevier, 2020, pp. 195–221.

[6] K. Wu, D. Su, J. Liu, R. Saha, and J.-P. Wang, "Magnetic nanoparticles in nanomedicine: a review of recent advances," *Nanotechnology*, vol. 30, no. 50, p. 502003, Sep. 2019, doi: 10.1088/1361-6528/ab4241.

[7] A. Farmany, S. S. Mortazavi, and H. Mahdavi, "Ultrasond-assisted synthesis of Fe3O4/SiO2 core/shell with enhanced adsorption capacity for diazinon removal," *Journal of Magnetism and Magnetic Materials*, vol. 416, pp. 75–80, Oct. 2016, doi: 10.1016/j.jmmm.2016.04.007.

[8] L. Li *et al.*, "Synthesis, Properties, and Environmental Applications of Nanoscale Iron-Based Materials: A Review," *Critical Reviews in Environmental Science and Technology*, vol. 36, no. 5, pp. 405–431, Oct. 2006, doi: 10.1080/10643380600620387.

[9] L. M. Martínez-Prieto *et al.*, "Ultrastable Magnetic Nanoparticles Encapsulated in Carbon for Magnetically Induced Catalysis," *ACS Appl. Nano Mater.*, vol. 3, no. 7, pp. 7076–7087, Jul. 2020, doi: 10.1021/acsanm.0c01392.

[10] X. Sun, Y. Huang, and D. E. Nikles, "FePt and CoPt magnetic nanoparticles film for future high density data storage media," *International Journal of Nanotechnology*, vol. 1, no. 3, pp. 328–346, Jan. 2004, doi: 10.1504/IJNT.2004.004914.

[11] C. Bai, H. Zhang, L. Zeng, X. Zhao, and L. Ma, "Inductive Magnetic Nanoparticle Sensor Based on Microfluidic Chip Oil Detection Technology," *Micromachines*, vol. 11, no. 2, Art. no. 2, Feb. 2020, doi: 10.3390/mi11020183.

[12] S. L, W. F, W. Y, Z. F, X. J, and M. L, "A novel method to detect Listeria monocytogenes via superparamagnetic lateral flow immunoassay.," *Anal Bioanal Chem*, vol. 407, no. 2, pp. 529–535, Dec. 2014, doi: 10.1007/s00216-014-8276-8.

[13] Y. Liu *et al.*, "A highly sensitive and flexible magnetic nanoprobe labeled immunochromatographic assay platform for pathogen Vibrio parahaemolyticus," *International Journal of Food Microbiology*, vol. 211, pp. 109–116, Oct. 2015, doi: 10.1016/j.ijfoodmicro.2015.07.005.

[14] D. Serrate *et al.*, "Quantitative biomolecular sensing station based on magnetoresistive patterned arrays," *Biosens Bioelectron*, vol. 35, no. 1, pp. 206–212, May 2012, doi: 10.1016/j.bios.2012.02.048.

[15] H. Lei, K. Wang, X. Ji, and D. Cui, "Contactless Measurement of Magnetic Nanoparticles on Lateral Flow Strips Using Tunneling Magnetoresistance (TMR) Sensors in Differential Configuration," *Sensors*, vol. 16, no. 12, Art. no. 12, Dec. 2016, doi: 10.3390/s16122130.

[16] X.-H. Mu *et al.*, "A new rapid detection method for ricin based on tunneling magnetoresistance biosensor," *Sensors and Actuators B: Chemical*, vol. 284, pp. 638–649, Apr. 2019, doi: 10.1016/j.snb.2018.12.127.

[17] C. Ren, Q. Bayin, S. Feng, Y. Fu, X. Ma, and J. Guo, "Biomarkers detection with magnetoresistance-based sensors," *Biosensors and Bioelectronics*, vol. 165, p. 112340, Oct. 2020, doi: 10.1016/j.bios.2020.112340.

[18] M. Sekino *et al.*, "Handheld magnetic probe with permanent magnet and Hall sensor for identifying sentinel lymph nodes in breast cancer patients," *Scientific Reports*, vol. 8, no. 1, Art. no. 1, Jan. 2018, doi: 10.1038/s41598-018-19480-1.

[19] P. Liu, K. Skucha, M. Megens, and B. Boser, "A CMOS Hall-Effect Sensor for the Characterization and Detection of Magnetic Nanoparticles for Biomedical Applications," *IEEE Transactions on Magnetics*, vol. 47, no. 10, pp. 3449–3451, Oct. 2011, doi: 10.1109/TMAG.2011.2158600.

[20] H. A. Ferreira, D. L. Graham, P. P. Freitas, and J. M. S. Cabral, "Biodetection using magnetically labeled biomolecules and arrays of spin valve sensors (invited)," *Journal of Applied Physics*, vol. 93, no. 10, pp. 7281–7286, May 2003, doi: 10.1063/1.1544449.

[21] K. Enpuku, Y. Tsujita, K. Nakamura, T. Sasayama, and T. Yoshida, "Biosensing utilizing magnetic markers and superconducting quantum interference devices," *Supercond. Sci. Technol.*, vol. 30, no. 5, p. 053002, Mar. 2017, doi: 10.1088/1361-6668/aa5fce.

[22] A. Moyano, E. Serrano-Pertierra, M. Salvador, J. Martínez-García, M. Rivas, and M. C. Blanco-López, "Magnetic Lateral Flow Immunoassays," *Diagnostics*, vol. 10, p. 288, May 2020, doi: 10.3390/diagnostics10050288.

[23] Z. Yang, Y. Liu, C. Lei, X. Sun, and Y. Zhou, "A flexible giant magnetoimpedance-based biosensor for the determination of the biomarker C-reactive protein," *Microchim Acta*, vol. 182, no. 15, pp. 2411–2417, Nov. 2015, doi: 10.1007/s00604-015-1587-4.

[24] G. V. Kurlyandskaya, M. L. Sánchez, B. Hernando, V. M. Prida, P. Gorria, and M. Tejedor, "Giant-magnetoimpedance-based sensitive element as a model for biosensors," *Appl. Phys. Lett.*, vol. 82, no. 18, pp. 3053–3055, May 2003, doi: 10.1063/1.1571957.

[25] M. Knobel, M. Vázquez, and L. Kraus, "Giant Magnetoimpedance," in *Handbook of Magnetic Materials*, vol. 15, Elsevier, 2003, pp. 497–563.

[26] T. Wang, Z. Yang, C. Lei, J. Lei, and Y. Zhou, "An integrated giant magnetoimpedance biosensor for detection of biomarker," *Biosensors and Bioelectronics*, vol. 58, pp. 338–344, Aug. 2014, doi: 10.1016/j.bios.2014.03.008.

[27] F. A. Blyakhman *et al.*, "Detection of Magnetic Nanoparticles in Blood Vessels," *Inorg. Mater. Appl. Res.*, vol. 11, no. 4, pp. 766–771, Jul. 2020, doi: 10.1134/S2075113320040061.

[28] A. Amirabadizadeh, Z. Lotfollahi, and A. Zelati, "Giant magnetoimpedance effect of Co68.15 Fe4.35 Si12.5 B15 amorphous wire in the presence of magnetite ferrofluid," *Journal of Magnetism and Magnetic Materials*, vol. 415, pp. 102–105, Oct. 2016, doi: 10.1016/j.jmmm.2015.11.029.

[29] H. Chiriac, D.-D. Herea, and S. Corodeanu, "Microwire array for giant magneto-impedance detection of magnetic particles for biosensor prototype," *Journal of Magnetism and Magnetic Materials*, vol. 311, no. 1, pp. 425–428, Apr. 2007, doi: 10.1016/j.jmmm.2006.11.207.

[30] G. V. Kurlyandskaya *et al.*, "Giant magnetoimpedance biosensor for ferrogel detection: Model system to evaluate properties of natural tissue," *Appl. Phys. Lett.*, vol. 106, no. 19, p. 193702, May 2015, doi: 10.1063/1.4921224.

[31] A. A. Yuvchenko, V. N. Lepalovskii, V. O. Vas'kovskii, A. P. Safronov, S. O. Volchkov, and G. V. Kurlyandskaya, "Magnetic impedance of structured film meanders in the presence of magnetic micro- and nanoparticles," *Tech. Phys.*, vol. 59, no. 2, pp. 230–236, Feb. 2014, doi: 10.1134/S1063784214020248.

[32] N. A. Buznikov *et al.*, "Modelling of magnetoimpedance response of thin film sensitive element in the presence of ferrogel: Next step toward development of biosensor for in-tissue embedded magnetic nanoparticles detection," *Biosensors and Bioelectronics*, vol. 117, pp. 366–372, Oct. 2018, doi: 10.1016/j.bios.2018.06.032.

[33] A. García-Arribas *et al.*, "GMI detection of magnetic-particle concentration in continuous flow," *Sensors and Actuators A: Physical*, vol. 172, no. 1, pp. 103–108, Dec. 2011, doi: 10.1016/j.sna.2011.02.050.

[34] J. G. S. Duque, A. E. P. de Araujo, M. Knobel, A. Yelon, and P. Ciureanu, "Large nonlinear magnetoimpedance in amorphous Co80.89Fe4.38Si8.69B1.52Nb4.52 fibers," *Appl. Phys. Lett.*, vol. 83, no. 1, pp. 99–101, Jun. 2003, doi: 10.1063/1.1590435.

[35] D. Seddaoui, D. Menard, and A. Yelon, "Measurement and Model of the Tensile Stress Dependence of the Second Harmonic of Nonlinear GMI in Amorphous Wires," *IEEE Transactions on Magnetics*, vol. 43, no. 6, pp. 2986–2988, Jun. 2007, doi: 10.1109/TMAG.2007.893799.

[36] S. Atalay, P. Ripka, and N. Bayri, "Coil-less fluxgate effect in (Co0.94Fe0.06)72.5Si12.5B15 amorphous wires," *Journal of Magnetism and Magnetic Materials*, vol. 322, no. 15, pp. 2238–2243, Aug. 2010, doi: 10.1016/j.jmmm.2010.02.018.
[37] M. Butta, "Orthogonal Fluxgate Magnetometers," in *High Sensitivity Magnetometers*, A. Grosz, M. J. Haji-Sheikh, and S. C. Mukhopadhyay, Eds. Cham: Springer International Publishing, 2017, pp. 63–102.
[38] M. Butta, P. Ripka, J. P. Navarrete, and M. Vazquez, "Double Coil-Less Fluxgate in Bridge Configuration," *IEEE Transactions on Magnetics*, vol. 46, no. 2, pp. 532–535, Feb. 2010, doi: 10.1109/TMAG.2009.2033339.
[39] J. J. Beato-López, J. I. Pérez-Landazábal, and C. Gómez-Polo, "Magnetic nanoparticle detection method employing non-linear magnetoimpedance effects," *Journal of Applied Physics*, vol. 121, no. 16, p. 163901, Apr. 2017, doi: 10.1063/1.4981536.
[40] J. J. Beato-López, J. I. Pérez-Landazábal, and C. Gómez-Polo, "Enhanced Magnetic Nanoparticle Detection Sensitivity in Non-Linear Magnetoimpedance-Based Sensor," *IEEE Sensors Journal*, vol. 18, no. 21, pp. 8701–8708, Nov. 2018, doi: 10.1109/JSEN.2018.2868860.
[41] C. Cristea, M. Tertis, and R. Galatus, "Magnetic Nanoparticles for Antibiotics Detection," *Nanomaterials*, vol. 7, no. 6, Art. no. 6, Jun. 2017, doi: 10.3390/nano7060119.
[42] W. Zhao, J. Gu, L. Zhang, H. Chen, and J. Shi, "Fabrication of Uniform Magnetic Nanocomposite Spheres with a Magnetic Core/Mesoporous Silica Shell Structure," *J. Am. Chem. Soc.*, vol. 127, no. 25, pp. 8916–8917, Jun. 2005, doi: 10.1021/ja051113r.
[43] M. Benelmekki *et al.*, "Design and characterization of Ni2+ and Co2+ decorated Porous Magnetic Silica spheres synthesized by hydrothermal-assisted modified-Stöber method for His-tagged proteins separation," *Journal of Colloid and Interface Science*, vol. 365, no. 1, pp. 156–162, Jan. 2012, doi: 10.1016/j.jcis.2011.09.051.
[44] M.-H. Phan and H.-X. Peng, "Giant magnetoimpedance materials: Fundamentals and applications," *Progress in Materials Science*, vol. 53, no. 2, pp. 323–420, Feb. 2008, doi: 10.1016/j.pmatsci.2007.05.003.
[45] S. K. Pal, N. B. Manik, and A. Mitra, "Dependence of frequency and amplitude of the ac current on the GMI properties of Co based amorphous wires," *Materials Science and Engineering: A*, vol. 415, no. 1, pp. 195–201, Jan. 2006, doi: 10.1016/j.msea.2005.09.076.
[46] C. Gómez-Polo, M. Knobel, K. R. Pirota, and M. Vázquez, "Giant magnetoimpedance modelling using Fourier analysis in soft magnetic amorphous wires," *Physica B: Condensed Matter*, vol. 299, no. 3, pp. 322–328, Jun. 2001, doi: 10.1016/S0921-4526(01)00484-7.
[47] T. Wang, Y. Zhou, C. Lei, J. Lei, and Z. Yang, "Development of an ingenious method for determination of Dynabeads protein A based on a giant magnetoimpedance sensor," *Sensors and Actuators B: Chemical*, vol. 186, pp. 727–733, Sep. 2013, doi: 10.1016/j.snb.2013.06.052.

Figure 1: a) TEM micrographs and size distribution of MNPs. b) Room temperature hysteresis loop (*M-H*) of the magnetic nanoparticles. As the inset shows, the maximum applied magnetic field was 0.4T.

Figure 2. a) Top and b) cross-view of the detection configuration.

Figure 3. Functional block diagram of the employed electronics: (a) Voltage divider configuration for laboratory sensor characterization and (b) Proposed electronic design for the sensor.

Figure 4. Variation of the first harmonic voltage, V_{1f} with the applied magnetic field, *H*, for the set of MNPs samples, S1, S2, S3, and S4 ($\sigma = 0.007, 0.0021, 0.0035$ and $0.104\,{}^{mg}/_{mm^2}$ respectively) for a rotation angle (a) $\alpha = 0°$ and

(b) $\alpha = 180°$; (c) H_S field for maximum V_{1f} under both configurations. Inset: (a) V_{1f} versus *H* for the *sensor* and under the presence of *S4* sample, $\sigma = 0.104\,{}^{mg}/_{mm^2}$.

Figure5. Variation of the second harmonic voltage, V_{2f} with the applied magnetic field, *H* for the set of MNPs S1, S2, S3, and S4 ($\sigma = 0.007, 0.0021, 0.0035$ and $0.104\,{}^{mg}/_{mm^2}$ respectively), (a) at a rotation angle $\alpha = 0°$ and (b) H_S field at minimum V_{2f} under both configurations. The insets show (a) the curves obtained for the *sensor* and S4 in the whole *H* interval and (b) V_{2f} versus *H* for rotated $\alpha = 180°$ MNPs.

Figure 6. Magnetic field, H_S, for the maximum and minimum in V_{1f} and V_{2f}, respectively, as a function of σ for non-rotated MNPs. In the case of V_{2f} the response was also analyzed under a triangular signal excitation.

Figure 7. Variation of the first harmonic, V_{1f}, and second harmonic voltage, V_{2f} at *H = 0* as a function of (a) σ (for a fixed distance $d = d_0$), and (b) d under the effect of the S4 sample.

Figure 8. Schematic of the proposed electronic design.

Figure 9. Variation of the second harmonic voltage, V_0 measured by the electronic design at $H = 0$, for varying amount of MNPs, σ, over the sensor.

Figure 10. Detected variations of V_0 (second harmonic-electronic interface), as a function of distance d at null magnetic field and $\sigma = 0.104\,{}^{mg}/_{mm^2}$, ($m = 15mg$) for (**-**) the electronic interface and (**-**) V_{2f} voltage divider. Inset: Zoom of the V_{2f} variations for large d values region (electronic interface).

Figure 11. Variations of V_0 (second harmonic-electronic interface) as a function of distance d at null magnetic field and $\sigma = 0.007\,{}^{mg}/_{mm^2}$, ($m = 1mg$) for the electronic interface.

Tables

Table 1. Set of MNPs samples prepared for detection: MNP mass, *m*, and superficial density, *σ*.

CrediT authorship contribution statement

Juan Jesús Beato López: Conceptualization, Methodology, Measurements, Validation, Formal Analysis, Investigation, Data curation, Writing original draft and editing. **José María Algueta Miguel**: Development of electronic interface, Writing review, and editing. **Cristina Gómez Polo**: Conceptualization, Methodology, Formal Analysis, Data curation, Supervision, Resources, Funding acquisition, Writing review and editing.

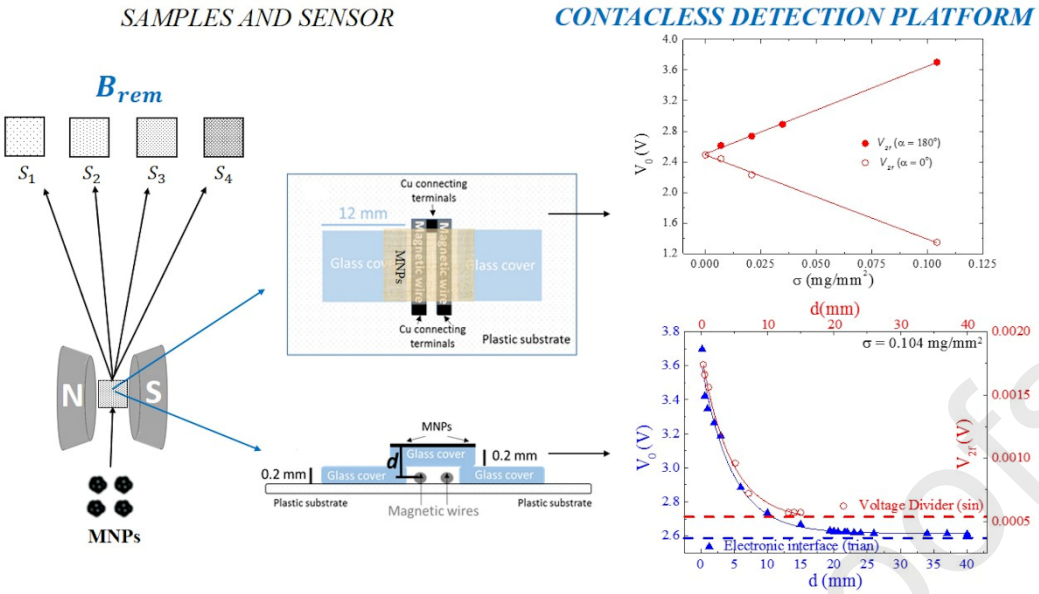

Contactless magnetic nanoparticle detection platform based on non-linear GMI effect

Juan Jesús Beato-López [1,2], José María Algueta-Miguel [3,4] and Cristina Gómez-Polo [1,2]*.

1 Departamento de Ciencias, Universidad Pública de Navarra, 31006 Pamplona, Spain

2 Institute for Advanced Materials and Mathematics INAMAT2, Universidad Pública de Navarra, 31006 Pamplona, Spain

3 Departamento de Ingeniería de Electricidad, Electrónica y Comunicación, Universidad Pública de Navarra, 31006 Pamplona, Spain

4 Institute of Smart Cities, Universidad Pública de Navarra, 31006 Pamplona, Spain

Corresponding autor: Juan Jesús Beato-López (juanjesus.beato@unavarra.es)

Highlights

- Analysis of the contactless detection procedure of magnetic (Fe_3O_4) nanoparticles.
- Non-linear GMI effect (first and second harmonic) as detection principle.
- Higher sensitivity displayed by the second harmonic voltage.
- Development of high sensitivity, low-cost, and contactless detection platform.

Declaration of interests

☒ The authors declare that they have no known competing financial interests or personal relationships that could have appeared to influence the work reported in this paper.

☐The authors declare the following financial interests/personal relationships which may be considered as potential competing interests: